

Silver Surface Iodination for Enhancing the Conductivity of Conductive Composites

By Cheng Yang,* Yu-Tao Xie, Matthew Ming-Fai Yuen,* Bing Xu, Bo Gao, Xiaomin Xiong, and C. P. Wong*

The electrical conductivity of a silver microflake-filled conductive composites is dramatically improved after a filler surface treatment. By a simple iodine solution treatment, nonstoichiometric silver/silver iodide nanoislands form on the silver filler surface. Evidence of the decrease of surface silver oxide species is provided by TOF-SIMS and the redox property of the nanoclusters is studied using cyclic voltammetry and TOF-SIMS depth profile analyses. The redox property of the nanoclusters on silver flakes helps enhance the electrical conductivity of the conductive composites. The electrical resistivity of the improved conductive composites is measured by four-point probe method; the reliability of the printed thin film resistors is evaluated by both the 85 °C/85% relative humidity moisture exposure and the -40 ~ 125 °C thermal cycling exposure. The conductive composite printed radio frequency identification (RFID) antennas with 27.5 wt% of the modified silver flake content show comparable performance in the RFID tag read range versus copper foil antennas, and better than those commercial conductive adhesives that require much higher silver content (i.e., 80 wt%). This work suggests that a surface chemistry method can significantly reduce the percolation threshold of the loading level of the silver flakes and improve the electrical conductivity of an important printed electronic passive component.

1. Introduction

In consumer electronics, electrically conductive adhesives (ECAs) are widely applied in both traditional interconnect applications as well as thin film plastic electronics: as compared to

solders, ECAs are environmentally friendly (no Pb), much simpler and faster for mass production (e.g., screen-printing and roll-to-roll printing), have a lower processing temperature (e.g., curing the resin dispersant at 150 °C or lower for a few minutes rather than fusing the Pb/Sn solder balls by reflowing within the furnace at 230 °C), and possess higher resolution in printing circuits (down to some 20 μm line width).^[1] Typical commercial polymer-based ECAs have high silver content: 70% ~ 85% by weight, or 20% ~ 37% by volume.^[2,3] Their overall electrical resistance is an aggregation of the local contact resistances of the conductive filler network (e.g., silver microflakes) in the resin dispersant.^[4] As a major concern, ECAs need to improve their electrical conductivity (usually ~10–4 Ω·cm) and reduce the cost to make them more competitive in the emerging printable electronics industry.

In a typical epoxy-based ECA, the low conductivity is subtly related to the surface status (such as metal oxidation) of

the fillers.^[5] On the other hand, the high melting point of the silver fillers makes it difficult to be annealed or sintered like the eutectic solder balls or nano-metal composed conductive inks.^[1,6,7] Thus the surface state of the conductive fillers, especially the inevitable oxidation of the filler surfaces, is a major disadvantage affecting the overall contact resistance.^[1,4,8–10] Because the resistivity of Ag₂O is 6 × 10¹⁶ times higher than silver metal, even a very thin layer of silver oxide covering the silver fillers can seriously impair the overall conductivity of the composites.^[5] In order to reduce the contact resistance of the ECAs at moderate curing conditions, adding reductive materials to inhibit the effect of silver oxidization might be a feasible method, as has been demonstrated by Li et al.^[11] However, the desorption of the nonconductive organic molecules from the silver metal surface usually involves elevated temperature.

As the percolation efficiency of the silver fillers is a critical issue for predicting the performance of the conductivity of ECAs,^[12,13] the silver flakes that we selected for use have an average diameter of 6 μm and an average thickness of 500 nm, which have a higher anisotropy (Figure 1a) than those in many commercial adhesives, giving them the opportunity to achieve a lower percolation threshold. Based on our experiments (four-point probe resistance test for printed resistors), the resistivity of the ECA samples prepared using 75 wt% of these

[*] Dr. C. Yang, Prof. M. M. F. Yuen, B. Gao
Department of Mechanical Engineering
The Hong Kong University of Science and Technology
Clear Water Bay, HK SAR (China)
E-mail: meymf@ust.hk

Dr. C. Yang, Dr. Y. T. Xie, Prof. B. Xu
Department of Chemistry
The Hong Kong University of Science and Technology
Clear Water Bay, HK SAR (China)
E-mail: yangch@ust.hk

Prof. X. Xiong
Department of Physics
Sun Yet-sen University
Guangzhou (China)

Prof. C. P. Wong
School of Materials Science and Engineering
Georgia Institute of Technology
771 Ferst Drive, N.W., Atlanta, GA 30332-0245 (USA)
E-mail: cp.wong@mse.gatech.edu

DOI: 10.1002/adfm.201000673

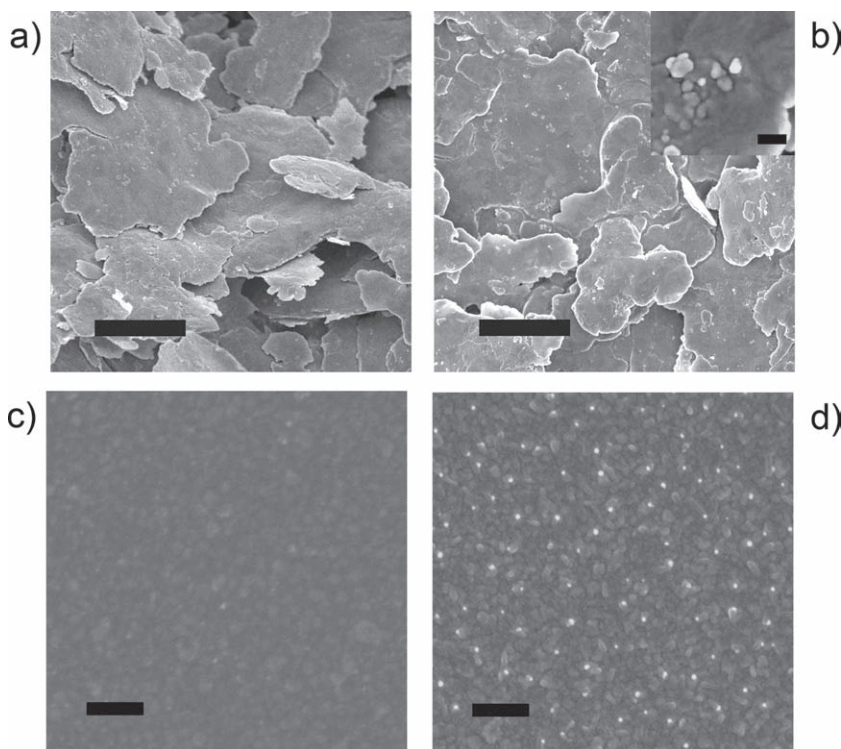


Figure 1. SEM images of the silver microflake samples and sputtered wafer samples before and after iodine modification. a) Original bare silver microflake sample. b) Iodine modified silver microflake sample (A3). a,b) Scale bar = 1 μm . Inset) Nanoislands on the same sample, scale bar = 100 nm. c) Original silver sputtered silicon wafer. d) Silver sputtered silicon wafer after dipped in an iodine solution (0.5 μM) for treatment. c,d) Scale bars = 500 nm.

as-obtained bare silver flakes reached $2.1 \times 10^{-4} \Omega \cdot \text{cm}$. However, when the filler amount of the ECAs is slightly reduced to 70 wt% (using the same bare silver flakes), the resistivity was higher than $10^{-3} \Omega \cdot \text{cm}$, which is too high for microelectronic applications.

Herein we introduce a novel iodination method to activate the silver filler surface. As iodination can effectively convert the non-conductive silver oxide to silver iodide, and the unique property of silver iodide can result in surface displacements, reconstruction effects, and redox process, etc.,^[14–17] we conducted a series of experiments including materials characterizations and systematically evaluated the improved ECAs using this new treatment method (Scheme 1). The modified silver fillers in the ECAs can develop stable metallic connections at moderate curing conditions (i.e., 150 $^{\circ}\text{C}$ for 15 min to cure the resin dispersant) when the silver content is reduced to a very low level. The electrical resistivity of the modified ECA reached $4.81 \times 10^{-4} \Omega \cdot \text{cm}$ when filled with as low as 27.5 wt% of the modified silver filler, and $1.13 \times 10^{-5} \Omega \cdot \text{cm}$ when filled with 60 wt% of silver (better than solders).

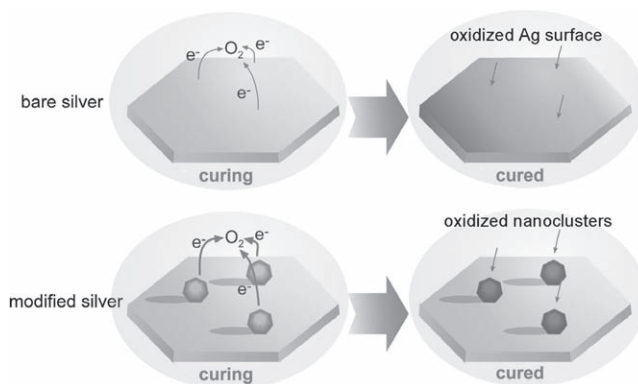
2. Results and Discussions

The iodination process is composed of a solution (ethanol) based treatment and subsequent filtration and vacuum drying. The morphology of the surface modified silver microflake samples was analyzed by scanning electron microscopy (SEM) on a JEOL 6700 field emission SEM (magnification $\times 20\,000$).

Herein, a series of different iodination conditions were carried out and the iodinated silver flake samples were marked as A1, A2, A3, etc. (see Supporting Information, Table S1). As shown in Figure 1b, we can clearly observe the nanoislands with an average size below 100 nm formed on the silver flake surface (silver/iodine = 500:1). As a parallel experiment for further detailed surface chemistry investigations, silver evaporated silicon wafers were used in this study as well (as shown in Figure 1c, d). Each wafer sample (1 cm^2) was immersed in ethanol solution in a very similar condition for the flake sample counterpart to precisely control the ratio between silver and iodine. Both samples showed similar morphological characters of the nanoislands, as shown in the SEM images. The formation of these nanoislands are analogous to previous reports of silver iodide formed on silver surface with very low iodine concentrations.^[17–23] Increasing the iodine content (e.g., elongating the solution processing time and the iodine concentration) results in the increase of both the size and density of the nanoislands on the silver surface (see Supporting Information, Figure S1).

In order to further characterize the iodinated silver surface including the nanoislands and other areas on silver surface, we carried out transmission electron microscopy–energy

dispersive X-ray spectroscopy (TEM-EDS) analysis on the cross sections of the fully cured ECA sample filled with 75 wt% of the silver filler (Figure 2). EDS analysis shows that silver is in excess amounts in both nanoislands A (Ag/I atomic ratio = 7.4:2.6) and B (Ag/I atomic ratio = 13.2:1.6), though the elemental ratio between silver and iodine in the nanoislands may vary. Although concentrated electron-beam irradiation may generate minor amount of silver nano-islands due to the damage of



Scheme 1. A schematic illustration showing the relatively stronger oxidation ability of the nanoclusters (particles) to the silver micro-flakes in the epoxy dispersant environment.

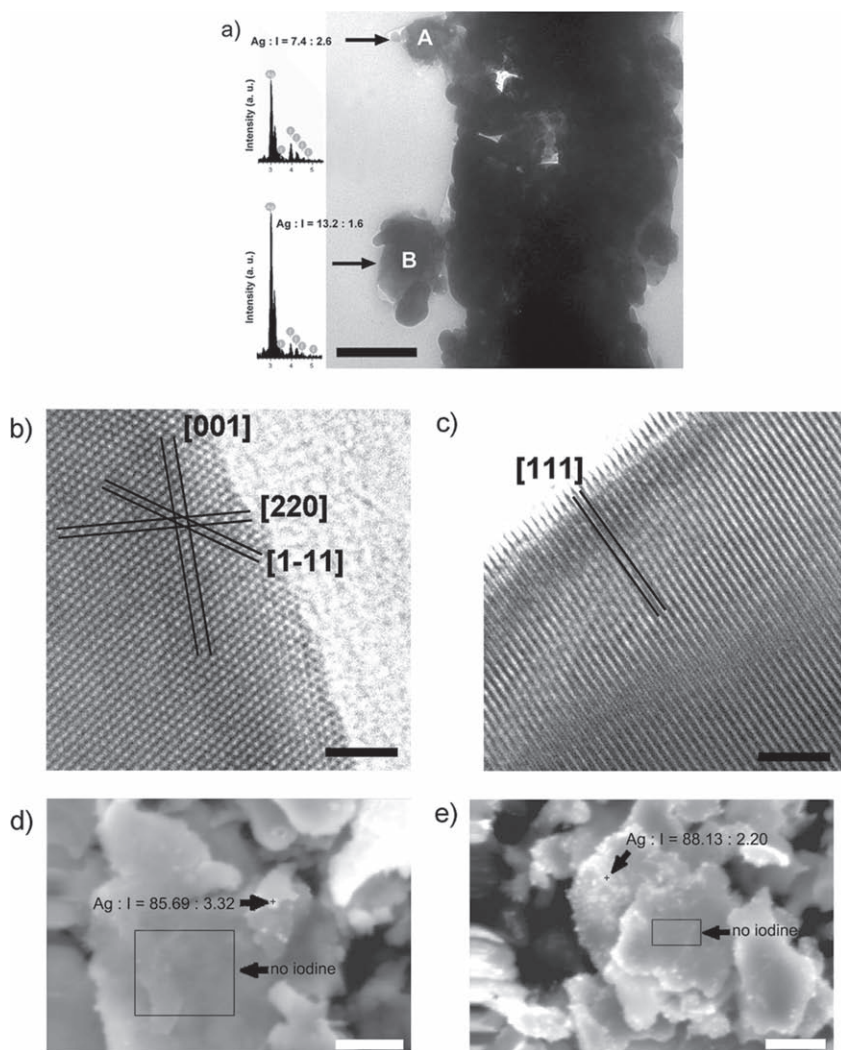


Figure 2. a–c) TEM-EDS analysis of ECA cross sections. **a)** TEM-EDS of the nanoislands on a sectioned ECA sample (filled with **A9**). Scale bar = 200 nm. EDS spectra are on the left. **b)** HRTEM image of bare silver microflake surface. Scale bar = 2 nm. **c)** HRTEM image of **A9** filled ECA surface, except for the nanocluster parts. Scale bar = 2 nm. The crystal lattice of silver metal is marked in both (b) and (c). (All samples are embedded in the resin filled with 75 wt% of the filler.) **d,e)** SEM-EDS analysis of the iodinated silver flakes. **d)** Sample **A3** and the selected area EDS elemental percent table; the elemental ratios between silver and iodine are listed in this image. Scale bar = 2.5 μm . **e)** Sample **A9** and the selected area EDS elemental percent table; the elemental ratios between silver and iodine are listed in this image. Scale bar = 2.5 μm .

AgI,^[24] care was taken to minimize this effect during the experiment. Those surface regions without nanoislands remained as pure crystalline silver metal, which is demonstrated in Figure 2b and 2c. The structural information from the crystalline lattice image showed that the iodine was only present in the nanoislands, which is consistent with the EDS analysis. SEM-EDS analysis of the **A3** and **A9** sample agreed with the TEM-EDS analysis, which suggested a limited distribution of the iodine-containing areas (Figure 2d and 2e). The above experimental observation suggests that the iodine containing areas are concentrated in the nanoislands areas and the silver content is stoichiometric excess in the nanoislands. Further analysis of the nanoislands by HRTEM was unsuccessful because of the

charging effect when these nanoislands are irradiated by concentrated electron beams. In these nanoislands, due to the nonstoichiometry, the abundant defect/fault sites facilitate the diffusion of silver atoms compared to the situation inside stoichiometric $\beta\text{-AgI}$ crystals, because of the further lowered 4d energy level for the Ag^+ (interstitial silver cations) as the lowest unoccupied molecular orbitals (LUMOs) in the AgI clusters,^[16] which facilitate the formation of more silver clusters inside the nanoislands.

To minimize the unpredictable interferences in surface analysis experiments, we conducted further investigations on the iodinated sputtered silver film on silicon wafer (the thickness of the silver foil is ~ 500 nm, which mimics the thickness of ordinary silver microflake fillers for an ECA instead of the commercial micrometer-sized silver flakes (Figure 1c and 1d). Four groups of samples were analyzed by time-of-flight secondary ion mass spectrometry (TOF-SIMS): 1) bare silver wafer, 2) sparsely covered by the nanoislands (1: Ag/I = 100:0.2) (resembling to the surface of **A3**), 3) moderately covered by the nanoislands (2: Ag/I = 100:0.4) (resembling to the surface of **A9**), 4) fully iodinated surface (3: Ag/I = 100:20), respectively. The sum of the relative peak intensities of $^{107}\text{Ag}_2\text{OH}^+$ and $^{107}\text{Ag}_2\text{O}^+$ over that of the silver base peak ($^{107}\text{Ag}^+$) is used as the index to demonstrate the overall oxidation level of the surface. After the curing and purging processes, the surface oxidation level of the unmodified bare silver sputtered wafer samples increased 15.5%, which suggests the oxidation of the silver surface in the curing process in the absence of Ag/AgI nanoclusters. The surface oxidation level of the modified silver decreased 60.4% in condition 1, and 54.3% in condition 2 (Figure 3a). This is the direct evidence that the Ag/AgI nanoclusters on the silver surface prevented the silver metal surface from oxidation in curing process. However, on the sputtered wafer sample that was fully iodinated (condition 3) (SEM images can be seen in the Supporting Information, Figure S1), the curing process incurred an increase of the total oxidation level. It seems that the curing process accelerated the oxidation of the remaining silver when the Ag/AgI nanoclusters fully covered the sample surface. Since the ratio of $(^{107}\text{Ag}_2\text{OH}^+ + ^{107}\text{Ag}_2\text{O}^+)/^{107}\text{Ag}^+$ is an index of the overall oxidation level of the sample surface, the less the nanoclusters covering the surface, the more fragment signals from the exposed silver metal surface were collected. For those samples with low and medium coverage levels of nanoclusters (conditions 1 and 2), after curing, the overall oxidation levels were lowered by 60% and 54%, respectively. Considering the surfaces of these

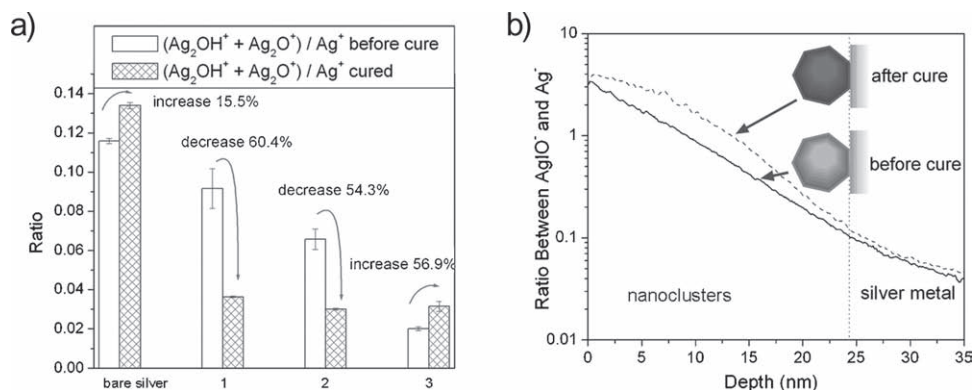


Figure 3. TOF-SIMS analysis of the silver sputtered silicon wafer samples. **a)** Silver sputtered silicon wafers after treatment of different concentration of iodine solutions. (The cured samples refer to those experienced a curing and post-washing process prior to this analysis.) Conditions: 1: Ag/I = 100:0.2; 2: Ag/I = 100:0.4; 3: Ag/I = 100:20. **b)** Depth profile of the surface-modified sputtered wafer sample (treatment condition: Ag/I = 100:20; y-axis in logarithmic scale).

two samples were partially covered by the nanoclusters, after the curing process, the oxidation of the silver surface (except for the nanoclusters) was greatly inhibited. It suggests that during the curing process, the nanoclusters influence oxygen adsorption on the silver surface and recover the part of the oxidized surface. This phenomenon may be attributed to excess amount of silver in the nanoclusters, which exhibited stronger reducing property than the bulk silver substrate.^[25,26]

Figure 3b demonstrates the situation of the silver surface when it is saturated by iodine treatment (Ag/I = 100:20, by atomic ratio). We tentatively partition the depth into two regions to facilitate the study of this spectrum: the left side illustrates the region of the nanoislands and the right side the region of the silver metal. In Figure 3b, this ratio ($^{107}\text{AgIO}^- / ^{107}\text{Ag}^-$) decreases with the sputtered depth, showing that the deeper the sputtering the stronger the collected substrate signals (i.e., $^{107}\text{Ag}^-$). After curing, this ratio ($^{107}\text{AgIO}^- / ^{107}\text{Ag}^-$) increased at the sample surface, which is about several nanometers in depth. For example, at the depth of ~7 nm, it is 1.1 times higher than the ratio of the sample before curing, showing that the nanoislands are further oxidized after curing. This is quite different from the TOF-SIMS analysis on a control sample of pure silver iodide crystalline powder (Aldrich, [7783-96-2], 99.999%), which shows negligible $^{107}\text{AgIO}^-$ peak intensity (ratio $\text{AgIO}^- / \text{Ag}^- = 6.3 \pm 0.88\%$). As an unstable and naturally rare substance, the observation of a large quantity of silver hyperiodite ($^{107}\text{AgIO}^-$) anions in the TOF-SIMS spectra indicates that in the nanocluster regions a large amount of oxygen incorporates into the Ag/AgI nanoislands.^[17,25–28] Comparison of the spectra before and after the mimic curing process demonstrates that the nanoislands are reactive to ambient oxygen and the curing process can accelerate the oxidation process. The interconversion between AgI and AgIO_x ($x = 1, 3$) species has been demonstrated to be a complicated charge transfer and oxidation process, which is related to many factors.^[29,30]

Further to the TOF-SIMS analysis, we recorded cyclic voltammograms on the iodine (condition 3) modified silver sputtered silicon wafer sample before and after the curing process (Figure 4). Subsequent to the curing process, a cyclic voltammogram was recorded on the iodine modified Ag from -0.6 to

+0.6 V (vs. SCE) in phosphorus buffer solution (PBS) (pH 7.0). The result is shown in Figure 4b. The Ag working electrode has an effective area of ~1 cm², which is stabilized at 0.3 V (vs. SCE) before the scan. The first cycle reveals that the anodic curve of Ag exhibits two anodic peaks at 0.221 V (vs. SCE) and -0.526 V (vs. SCE). According to literature,^[29,31] the first anodic peak at 0.221 V (vs. SCE) was related to the formation of I₂ from the reduction of IO₃⁻ on the Ag surface, which was different from the spectrum using a bare silver sputtered wafer as the electrode. The appearance of a peak at -0.526 V (vs. SCE) is due to the redox reaction $2\text{Ag}(s) \rightarrow 2\text{Ag} + \text{I}_2$.^[31,32] The second cycle displays two anodic peaks at -0.066 V (vs. SCE) and -0.458 V (vs. SCE). The anodic peak at -0.066 V (vs. SCE) is connected to the reduction of Ag₂O to Ag.^[33] Compared with the reduction peak of AgI in the first cycle, the anodic peak shifts to -0.458 V from -0.526 V (vs. SCE) in the second cycle. This was induced by the precipitated I₂, which was partially re-dissolved in PBS buffer. However, the peak at +0.221 V (vs. SCE) is not observed in the second cycle, nor in any cycle in the unmodified bare control sample or in a reversed scanning direction, as shown in Figure 4c and 4d, which indicates that the AgIO₃ structure was formed in the Ag/AgI nanoislands during the curing process and the Ag/AgI nanoislands exhibit a high electrochemical catalytic property to facilitate AgI to consume the oxygen to form AgIO₃ during the curing process.^[26] On the other hand, the silver microflakes cannot compete with the AgI in Ag/AgI nanoislands to be oxidized during the curing process because $E(\text{Ag}/\text{Ag}_2\text{O})$ (~-0.76 V) is smaller than $E(\text{AgI}/\text{AgIO}_3)$ (~-1.10 V). The analysis of the cyclic voltammograms is consistent with the observations in the TOF-SIMS spectra, which demonstrate that the surface oxidation process is localized in the Ag/AgI nanoislands during the curing process in an ECA. In the TOF-SIMS spectra, the fragment peak of AgIO⁻ is more dominant over that of AgIO₃⁻, due to the insensitivity of the relative large molecular weight of the latter. The interconversion between AgI and AgIO₃ has been demonstrated to be a complicated process among Ag-I species.^[29,30] The above cyclic voltammetry and TOF-SIMS analyses provide a second understanding of the profound reaction mechanism of the Ag/AgI oxidation process to supplement the previous works.^[28,29]

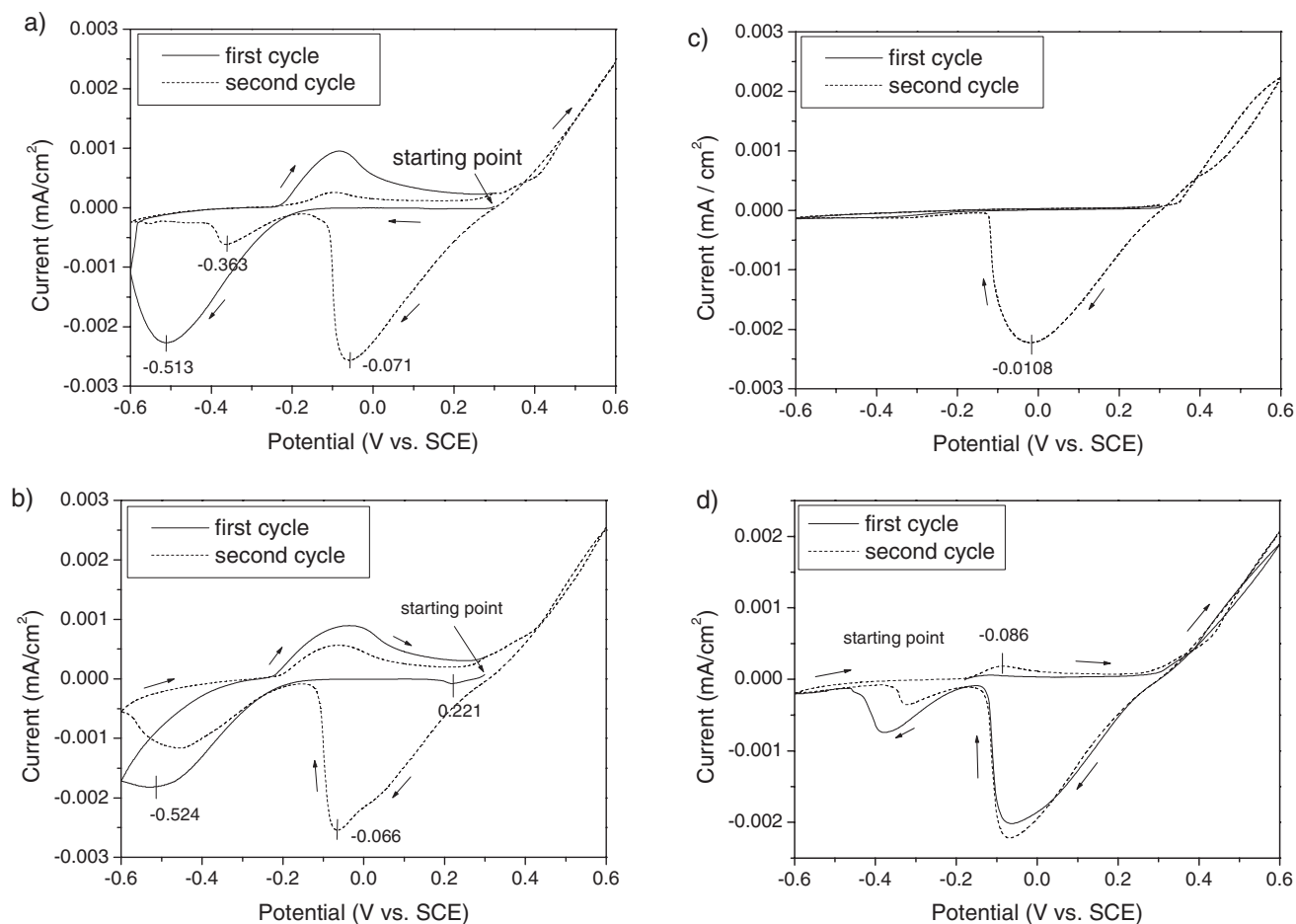


Figure 4. Cyclic voltammogram of the iodine modified wafer sample. (The scan starts at +0.3 V (vs. SCE) towards the negative direction in the limit between -0.6 V (vs. SCE) and $+0.6$ V (vs. SCE).) **a)** Iodinated silver sputtered wafer sample before the curing process. **b)** Wafer sample after a curing and post-washing process. **c)** Bare silver wafer sample. (The scan starts at +0.3 V (vs. SCE) towards the negative direction in the limit between -0.6 V (vs. SCE) and $+0.6$ V (vs. SCE).) **d)** Iodine modified silver wafer sample. (The scan starts at -0.18 V (vs. SCE) towards the positive direction in the limit between -0.6 V (vs. SCE) and $+0.6$ V (vs. SCE).)

In some circumstances, solution-based iodine treatment for silver can eliminate the silver oxide layers over the metal surface and further progressively react with the silver atoms inside the surface, resulting the formation of the nonstoichiometric Ag/AgI structure.^[34] On the other hand, earlier scanning tunneling microscopy (STM) and ab initio studies also show that at a very low iodination level, the chemisorbed iodine affects the structural and electronic properties of the metal surface and induces lateral displacement of silver atoms.^[35] The adsorption layer is weakly associated to the silver metal surface due to the crystalline mismatch,^[18] and they can go through structural changes and cover less areas when subjected to heat.^[36] When silver goes through a solution based iodination, those iodinated regions occupy active sites such as the terraces and steps of the silver surface more selectively, and experience a subsequent ripening process,^[17,18,28,37] leaving the remaining part a clean silver surface due to an electrochemical process,^[17,18] although the dynamic process still needs further investigation. Both the concentration and amount of iodine are crucial factors in determining the coverage and morphology of the nanoislands on

the silver surface. The covering rate of these nonstoichiometric nanoislands plays a key role in modulating the surface property of silver. Based on the TEM-EDS and SEM-EDS results, we did not observe the wide spread coverage of silver iodide species on the silver surface, which suggests that under optimum conditions for the best conductivity (i.e., when filled with A3), only a small fraction of the surface is covered by the nanoislands and the rest is bare silver metal. The excess amount of silver clusters inside the nanoislands can actively involve in the charge transfer process and facilitates the reconstruction of the silver surfaces.^[16] TOF-SIMS and cyclic voltammetry analyses suggest that oxygen is incorporated into the nanoislands (partially due to the decomposition of silver iodide and oxidation of silver clusters) and this may alter the oxidation of the silver surfaces. The redistribution of the silver surface species could alter the path to the oxidation of the silver surface, which may play a key role in reducing the contact resistance of the silver filler interfaces in the ECAs.

The improved electrical conductivity was confirmed based on a four-point probe method on the thin film ECA samples, which

are commonly used for testing printed electronic resistors. The ECA samples filled with **A3** showed the highest electrical conductivity among all listed conditions, e.g., **A1**, **A4**, **A5**, **A6**, and **A9**, etc., as shown in **Figure 5a** (this figure only shows the resistivity data of the ECA samples lower than $10^{-3} \Omega \cdot \text{cm}$). The **A3** filled ECA has a volume resistivity of $5.92 \times 10^{-5} \Omega \cdot \text{cm}$ with a silver filler content of 40 wt% (6.5% v/v). The volume resistivity increased to $4.81 \times 10^{-4} \Omega \cdot \text{cm}$ when the silver filler content decreased to 27.5 wt% (3.8% v/v). Further reduction of the filler content resulted in higher and unstable resistivity. For example, the resistivity of the ECA filled with 70 wt% of **A1** is only $1.51 \times 10^{-4} \Omega \cdot \text{cm}$ (not shown in this figure), and filled with 60 wt% of **A5** is only $2.99 \times 10^{-4} \Omega \cdot \text{cm}$, while the resistivity of the ECA filled with 70 wt% of **A3** is $6.90 \times 10^{-6} \Omega \cdot \text{cm}$, and filled with 60 wt% of **A3** is $1.13 \times 10^{-5} \Omega \cdot \text{cm}$. When further decreasing the content of **A3** in the ECAs to be lower than 27.5 wt%, i.e., 27 wt%, 26 wt%, 25 wt%, etc., from the SEM analysis of the bulk ECA samples, we observed sedimentations of the fillers, which is due to the mismatch of the density between silver microflakes and the epoxy resin (see Supporting Information, Figure S5). These sedimentations denote that when the silver filler content is

lower than 27 wt%, the silver fillers cannot form an associated network, which is crucial for electrical percolations. Even though this silver content is much lower than the theoretical percolation threshold, the ECA still exhibits excellent conductivity. This phenomenon suggests that the silver flakes are in an agglomeration status in the epoxy matrix instead of an ideally even distribution. Even though this sedimentation effect may have problems in omnidirectional percolation, the ultralow filler content ECAs all exhibit excellent 2D electrical conductivity in the form of printed thin film resistors, which will be discussed in the following paragraphs.

As another major concern for real application, the reliability performance of the ECA samples must be evaluated. Here the screen-printed resistor samples of the **A3**-filled ECA samples were used for both thermal-moisture and thermal impact examinations. In the first test, the **A3**-filled ECA samples were conditioned in a TERCHY MHU-150L humidity chamber (85 °C/85% relative humidity) for 720 h. The resistance of the samples was measured by a four-point probe test in each day during the test. The volume resistivity of each ECA sample showed negligible variations in the electrical resistivity in this

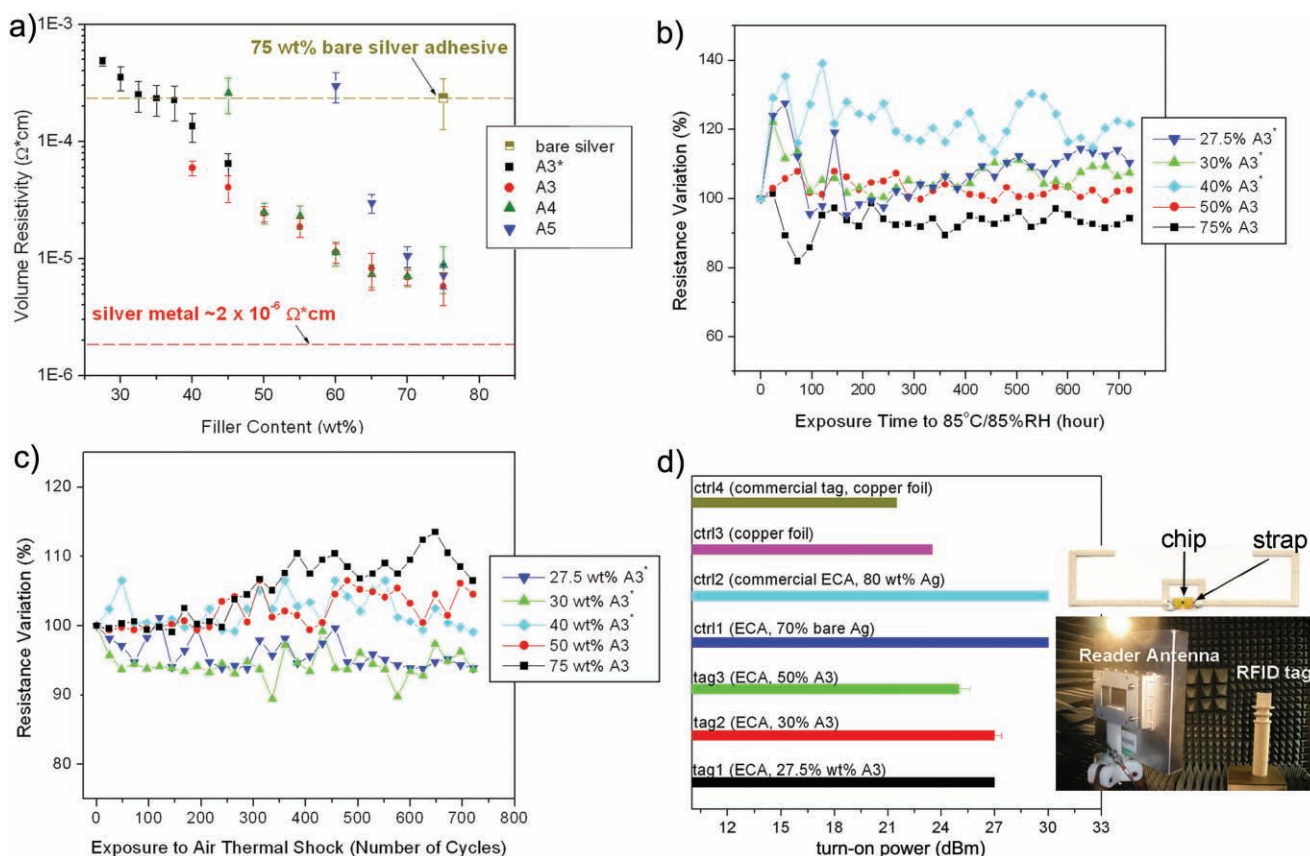


Figure 5. a) Volume resistivities of the modified ECAs and control with different silver filler contents. The iodine weight contents are listed on the right side of the legend. (*This series of data of **A3** filled ECAs are based on Novolac type epoxy resin to adjust the viscosity at low filler content.) b) The 85 °C/85% relative humidity reliability test (720 h) of some of the **A3** filled ECAs. (*This series of data of **A3** filled ECAs are based on Novolac type epoxy resin to adjust the viscosity at low filler content.) c) Thermal cycling reliability test (720 h) of some of the **A3** filled ECAs. (*This series of data of **A3** filled ECAs are based on Novolac type epoxy resin to adjust the viscosity at low filler content.) d) Read range test of the RFID tags. Turn on power measurement on the **A3** filled ECA RFID tag samples (**tag 1**, **2**, **3**) and the control samples (**ctrl 1**, **2**, **3**, **4**). Inset) A photographic image of the RFID tag prototype printed with the ECA containing 50 wt% of **A3**; a photographic image of the turn-on power test in an anechoic chamber. (The distance between RFID reader antenna and RFID tag is 1 m.)

temperature-humidity testing (THT) experiment (Figure 5b). Another set of the ECA samples was conditioned in an ESPEC chamber for the thermal cycling test (TCT) between -40 and 125 °C (JESD22-A104). The resistance data were obtained through a data logger connected to each of the ECA sample (Figure 5c). Both the THT and TCT test results suggest that the screen-printed resistors based on the A3-filled ECA have excellent reliability for real application.

We further demonstrated the feasibility of using them in printed electronics applications, i.e., printing ultrahigh frequency radio frequency identification (UHF RFID) tags; the signal transmission efficiency of these ultralow cost ECA printed tag antennas showed comparable performance to those copper-foil-etched antennas (copper-foil-based antenna, Class 1 Gen 2 RFID strap, Alien Tech. Inc.), which have a higher cost and may have environmental problems.^[38] The signal transmission performance of each RFID tag sample is displayed in Figure 5d. The minimum turn-on power of the reader was used to evaluate the signal transmission performance. In Figure 5d, we can observe that the printed tag antenna ECA filled with 27.5 wt% of the modified silver fillers (**tag1**, 27 dBm) and others with higher filler contents all exhibited better performance than **ctrl1**, which has ECA filled with 70 wt% of bare silver in the tag antenna (30 dBm). They also showed better performance than a control commercial ECA (**ctrl2**, 30 dBm), which contains 80 wt% of silver micro-flakes filled in the antenna. These read range results of the filler-modified ultralow cost RFID tags were just barely lower than those electrochemically etched metallic antennas (**ctrl3**, 23 dBm and **ctrl4**, 21.5 dBm). The result demonstrates that the A3 based ECAs are feasible and more cost-effective.

3. Conclusion

In summary, we present a novel surface iodination method that can significantly improve the electrical conductivity by lowering the silver percolation of the electrical conductive adhesives. TOF-SIMS, cyclic voltammetry, and TEM/SEM-EDS analyses demonstrate that nonstoichiometric Ag/AgI nanoislands sparsely form on silver surfaces due to this treatment. These nanoislands have a high tendency for oxygen incorporation, while the rest of the silver surface remains unaltered. At a low iodination condition, the coverage of the nanoisland on the silver surface is very minor and has no adverse effect to the surface conductivity. TOF-SIMS and cyclic voltammetry analyses suggest that the nanoislands are more easily oxidized than the bare silver surface and may cause competitive effects to activate the silver filler surface. Using this method, we adopted the surface-modified silver microflakes in common epoxy resin matrices and demonstrated the effectiveness in improving the conductive performance of the conductive composites with ultralow filler contents.^[39] With the modified silver filler content as low as 27.5 wt%, the conductive composites retain a resistivity as low as 4.81×10^{-4} Ω ·cm and exhibit excellent reliability. We believe this simple method by using surface iodination to develop metallic contact will have vast applications in consumer polymer electronics, such as those requiring ultralow

cost, low processing temperature, as well as high conductance and reliability.

4. Experimental Section

Preparation of the ECAs: Silver microflakes are from Chengdu Banknote Printing Complex, China (SF-01). We dispersed the microflakes in the ethanol solution of iodine for surface modification. The microflakes immediately reacted with iodine and after a simple precipitation the solution turned clear. We collected the surface-modified silver microflakes using a simple filtration method and dried them in vacuum. A control experiment for the bare silver flakes was carried out in an analogous method above in pure ethanol solution to eliminate any absorbent over the silver flakes. A subsequent mixing process was applied to these microflakes with resins and hardeners. Bisphenol-A type epoxy (Shell Epon 828) and methyltetrahydrophthalic anhydride (MTHPA, Lindau Chemicals) were used. The Novolac type epoxy resin used for low silver content formulation was an 8:2 (by weight) mixture of Kolon Industries KEP-1138 and Dow Chemicals D. E. R. 331. The ratio of epoxy to hardener was 1:1 by mole ratio based on the epoxide equivalent weight (EEW) of the epoxy resin and the hydroxyl equivalent weight (HEW) of the hardener. The catalyst was 2-ethyl,4-methyl imidazole and the concentration of the catalyst was 1 wt% to the resin. We mixed the pastes subsequently in a THINKY ARE 250 conditioning mixer of 2000 rpm for 8 min. Then we loaded the silver paste with a thickness of 20 μ m onto a piece of DuPont Melinex ST507 poly(ethylene terephthalate) (PET) film using a DEK-260 screen printer at a printing speed of 250 mm s^{-1} . Then within 30 min, the pastes were cured at 150 °C for 15 min. The thickness of the printed ECA samples on the PET film was confirmed using a caliper and a Surface Profile System, Model Alpha-Step 200 (Tencor) to ensure the range is within 25.4 ± 7 μ m.

Preparation and Modification of the Silver Sputtered Wafers: The sputtered wafers were prepared by sputtering silver onto a piece of silicon wafers (5 in.) using an ARC-12M sputtering system (DC sputtering power source: 2×250 W, Chamber pressure: 5×10^{-6} torr, sputtering rate: 190 \AA s^{-1}). The thickness of the sputtered silver is 5000 \AA . The wafers were cut into small pieces of 1 cm^2 and then dipped in the ethanol solution of iodine with different concentrations. In order to study the affects of the cure process towards the silver surface, we immersed the wafers into a mixture of bisphenol-A (Epon 828) and hardener MTHPA (mole ratio = 1:1) and then heated the samples at 150 °C for 15 min (same condition for curing the ECAs). Subsequently, we carefully purged the samples with acetone and ethanol until all resin residues were removed. (From TOF-SIMS analysis, no resin residues were observed in all sputtered wafers, showing the purging process was effective).

Characterization: A JEOL 6700F field emission SEM at 8 kV and a JEOL 6390 SEM at 15 kV, equipped with an EDS (Bruker AXS model xFlas Detector 4010), were used to study the silver microflakes and silver sputtered silicon wafers. A TEM (JEOL 2010 accompanied with an OXFORD Inca EnergyTEM200 EDS system) was used to analyze the of the ECA sections. The sections were prepared by using a Leica ultracut-R ultra-microtome, with a cutting speed at 1 mm s^{-1} and thickness of 60 nm. TOF-SIMS (Model TOFSIMSV, ION-TOF) was used to characterize the surface of the sputtered wafer samples. The volume resistivities of the ECA samples were measured on a Jandel 4-point probe tester. The thickness of the samples were 24 ± 5 μ m (same to the antennas). The derivation of the resistivity was based on

$$\rho = \frac{\pi t}{\ln 2} \left(\frac{V}{I} \right) \quad (1)$$

where t is the thickness, and V and I are the applied potential and the measured current, respectively.

The cyclic voltammetry experiments were carried out on a three-electrode system, consisting of a silver working electrode, a reference

electrode, and a counter electrode. The working electrode was a piece of Ag-sputtered silicon wafer square with the immersed dimension of 1 cm². The reference electrode was a saturated calomel electrode (SCE). A CHI660A electrochemical workstation was used to control and measure potentials and to record current responses. Experiments were conducted at room temperature in an aqueous NaH₂PO₄ solution (0.02 M) with the pH adjusted to 7.0. All experiments started at +0.3 V and scans started towards the anodic direction at the rate of 0.05 V s⁻¹. Then the scan reversed at -0.6 V and next ones were set between the limit of -0.6 V and +0.6 V.

The volume resistivity of the ECA samples was measured according to ASTM F1896-98. The ECA samples were conditioned in a TERCHY MHU-150L humidity chamber (85 °C/85% relative humidity) for 720 h for the temperature-humidity testing (THT). Another set of the same sample was conditioned in an ESPEC chamber model EGNZ12-6CWL for the thermal cycling test (TCT) between -40 and 125 °C (JESD22-A104). We attached a piece of Class 1 Gen 2 RFID chip (Alien Technology Inc.) to the center of the ECA printed antenna using ABLEBOND 84-1A, then we analyzed the read range of the tags by using a commercial UHF RFID system (CSL CS461) in an anechoic chamber with a fixed reader-to-tag distance of 1 m. The copper foil based tag antenna sample (**ctrl2**) was prepared by etching the copper clad.

Supporting Information

Supporting Information is available online from Wiley InterScience or from the author.

Acknowledgements

We acknowledge the funding from ITF GHP/032/05 (Hong Kong).

Received: April 8, 2010

Published online: July 6, 2010

- [1] Y. Li, K. S. Moon, C. P. Wong, *Science* **2005**, *308*, 1419.
- [2] L. R. Bao, B. Wei, A. Y. Xiao, *IEEE Electron. Compon. Technol. Conf.* **2007**, *57*, 494.
- [3] D. Stauffer, A. Aharony, *Introduction to Percolation Theory*, 2nd ed., Taylor & Francis, LondonUK **1992**, Ch. 1.
- [4] R. Strumpler, J. Glatz-Reichenbach, *J. Electroceram.* **1999**, *3*, 329.
- [5] K. Chatterjee, S. Banerjee, D. Chakravorty, *Europhys. Lett.* **2004**, *66*, 592.
- [6] J. Liu, *Conductive Adhesives for Electronics Packaging*, Electrochemical Publications, Port Erin, Isle of Man, UK **1999**
- [7] H. J. Jiang, K. S. Moon, Y. Li, C. P. Wong, *Chem. Mater.* **2006**, *18*, 2969.
- [8] S. Sivaramakrishnan, P. J. Chia, Y. C. Yeo, L. L. Chua, P. K. H. Ho, *Nat. Mater.* **2007**, *6*, 149.
- [9] C. Yang, B. Xu, M. M. F. Yuen, *58th IEEE Electron. Compon. Technol. Conf.* **2008**, *5*, 213.
- [10] G. R. Ruschau, S. Yoshikawa, R. E. Newnham, *J. Appl. Phys.* **1992**, *72*, 953.
- [11] Y. Li, A. Whitman, K. S. Moon, C. P. Wong, *Proc. Electron. Compon. Technol. Conf.* **2005**, *2*, 1648.
- [12] Y. B. Yi, *Phys. Rev. E* **2006**, *74*, 031112.
- [13] Y. B. Yi, E. Tawerghi, *Phys. Rev. E* **2009**, *79*, 041134.
- [14] P. Boolchand, W. J. Bresser, *Nature* **2001**, *410*, 1070.
- [15] M. Tatsumisago, Y. Shinkuma, T. Minami, *Nature* **1991**, *354*, 217.
- [16] K. Matsunaga, I. Tanaka, H. Adachi, *J. Phys. Soc. Jpn.* **1998**, *67*, 2027.
- [17] U. Hasse, S. Fletcher, F. Scholz, *J. Solid State Electrochem.* **2006**, *10*, 833.
- [18] B. V. Andryushechkin, G. M. Zhidomirov, K. N. Eltsov, Y. V. Hladchanka, A. A. Korlyukov, *Phys. Rev. B* **2009**, *80*, 10.
- [19] U. Hasse, F. Scholz, *Electrochem. Commun.* **2004**, *6*, 409.
- [20] B. Wiley, Y. G. Sun, Y. Xia, *Acc. Chem. Res.* **2007**, *40*, 1067.
- [21] P. L. Redmond, A. J. Hallock, L. E. Brus, *Nano Lett.* **2005**, *5*, 131.
- [22] Y. G. Sun, B. Mayers, T. Herricks, Y. N. Xia, *Nano Lett.* **2003**, *3*, 955.
- [23] Y. L. Wang, P. H. C. Camargo, S. E. Skrabalak, H. C. Gu, Y. N. Xia, *Langmuir* **2008**, *24*, 12042.
- [24] R. W. Horne, M. N. McMorris, R. H. Ottewill, *J. Photogr. Sci.* **1962**, *10*, 235.
- [25] V. Bonacic-Koutecky, R. Mitric, *Chem. Rev.* **2005**, *105*, 11.
- [26] J. Hagen, L. D. Socaciu, J. Le Roux, D. Popolan, T. M. Bernhardt, L. Woste, R. Mitric, H. Noack, V. Bonacic-Koutecky, *J. Am. Chem. Soc.* **2004**, *126*, 3442.
- [27] M. S. Sibbald, G. Chumanov, T. M. Cotton, *J. Electroanal. Chem.* **1997**, *438*, 179.
- [28] X. Zhang, S. Stewart, D. W. Shoesmith, J. C. Wren, *J. Electrochem. Soc.* **2007**, *154*, F70.
- [29] F. Fourcade, T. Tzedakis, A. Bergel, *Chem. Eng. Sci.* **2003**, *58*, 3507.
- [30] K. C. Patil, C. N. R. Rao, Lackson, Jw, C. E. Dryden, *J. Inorg. Nucl. Chem.* **1967**, *29*, 407.
- [31] A. J. Bard, R. Parsons, J. Jordan, *Standard Potentials in Aqueous Solution*, Marcell Dekker, Inc., New York **1985**
- [32] K. Arai, F. Kusu, N. Noguchi, K. Takamura, H. Osawa, *Anal. Biochem.* **1996**, *240*, 109.
- [33] M. Hepel, M. Tomkiewicz, *J. Electrochem. Soc.* **1984**, *131*, 1288.
- [34] P. S. Kumar, C. S. Sunandana, *Proc. SPIE* **2001**, *4807*, 241.
- [35] Y. Wang, Q. Sun, K. N. Fan, J. F. Deng, *Chem. Phys. Lett.* **2001**, *334*, 411.
- [36] U. Bardi, G. Rovida, *Surf. Sci.* **1983**, *128*, 145.
- [37] P. A. Thiel, M. Shen, D. J. Liu, J. W. Evans, *J. Phys. Chem. C* **2009**, *113*, 5047.
- [38] P. V. Nikitin, S. Lam, K. V. S. Rao, *IEEE Antennas and Propagation Society International Symposium*, **2005**, *2B*, 353.
- [39] The addition level of iodine (halogen) content is compatible with electronics industry standard, IEC 61249-2-21, for the requirements of halogen free materials.